Journal of Molecular Catalysis A: Chemical 367 (2013) 38–45

Contents lists available at SciVerse ScienceDirect

Journal of Molecular Catalysis A: Chemical

journal homepage: www.elsevier.com/locate/molcata

Catalytic conversion of syngas into C_{2+} oxygenates over Rh/SiO_2-based catalysts: The remarkable effect of hydroxyls on the SiO_2

Jun Yu [a,b], Dongsen Mao [b,*], Lupeng Han [b], Qiangsheng Guo [b], Guanzhong Lu [a,b,**]

[a] Key Laboratory for Advanced Material and Research Institute of Industrial Catalysis, East China University of Science and Technology, Shanghai 200237, PR China
[b] Research Institute of Applied Catalysis, School of Chemical and Environmental Engineering, Shanghai Institute of Technology, Shanghai 201418, PR China

ARTICLE INFO

Article history:
Received 23 June 2012
Received in revised form 12 October 2012
Accepted 18 October 2012
Available online 10 November 2012

Keywords:
SiO_2
Rh-based catalyst
CO hydrogenation
C_{2+} oxygenates
FT-IR

ABSTRACT

A series of Rh–Mn–Li catalysts supported on SiO_2 prepared by different methods were tested for the synthesis of C_{2+} oxygenates via CO hydrogenation. The catalysts were comprehensively characterized by N_2 adsorption–desorption, XRD, in situ FT-IR, CO-TPD, TPSR, and H_2-TPR. It was found that the Rh–Mn–Li catalyst supported on the SiO_2 synthesized by the Stöber method exhibited the highest CO conversion and selectivity toward C_{2+} oxygenates compared with other catalysts. The investigation based on the catalytic performance and characterizations of the catalysts suggests that the hydroxyl–metal interaction over the catalysts supported on different SiO_2 results in different desorption behavior of the adsorbed CO. The specific interaction between the active components and weakly H-bonded hydroxyls on the SiO_2 prepared by the Stöber method promoted the transformation from $Rh^+(CO)_2$ to Rh–CO and facilitated the desorption/reactivity of adsorbed CO as a function of temperature in the presence of hydrogen, which were proposed to be the crucial factors for obtaining higher CO conversion and C_{2+} oxygenates selectivity.

1. Introduction

The synthesis of ethanol and other C_2 oxygenates (e.g., acetaldehyde and acetic acid) from syngas ($CO + H_2$), which was derived from coal or biomass, has attracted much attention in recent years because it can decrease the global dependence on petroleum [1–4]. In spite of the continuous amount of research on this catalytic conversion route, no commercial process exists due to the relatively low selectivity and yield of C_2 oxygenates using most known catalysts [1]. Therefore, it is essential to develop more effective catalysts for this catalytic process.

Rh-based catalysts have been known to be the most efficient ones in the synthesis of C_2 oxygenates from CO hydrogenation due to their unique CO adsorption behavior [5–12]. The influence of various supports on the catalytic activity of Rh-based catalysts has been widely investigated [13–19]. SiO_2 has been the most frequently used support, since the Rh-based catalysts supported on it usually exhibit moderate activity and good selectivity toward C_2 oxygenates from CO hydrogenation. Furthermore, the different properties of SiO_2 have a considerable influence on the Rh-based catalysts, which finally leads to disparities in the catalytic performance [20–24]. For example, Chen et al. [21] observed that the crystallite size distribution was narrower and Rh particles were more homogeneously dispersed when 14–20 mesh silica was used instead of 20–40 mesh as a support for Rh–Mn–Li catalyst. As a result, the space time yield (STY) and selectivity of C_{2+} oxygenates were significantly increased from 338.6 g/(kg h) and 49.2% to 618.4 g/(kg h) and 54.6%, respectively ($T = 300\,^{\circ}C$, $P = 3$ MPa, $SV = 12{,}500\ h^{-1}$). Treatment of silica support with nC_1–C_5 alcohols also resulted in an enhancement of the STY of C_2 oxygenates by 10–30% depending on the specific alcohol [22]. This enhancement was attributed to the improved Rh dispersion and the increased ratio of Rh^+/Rh^0 sites on the catalyst surface, which facilitated the CO insertion reaction. Moreover, it is also considered that surface hydroxyl groups on silica play an important role in the structural rearrangement of the metal aggregates and the change in the oxidation state of the metal. Solymosi et al. [23] proposed that Rh^+ was most probably formed via an oxidation of the Rh^0 clusters by the surface OH groups of SiO_2. Basu et al. [24] reported that specific OH groups on Al_2O_3 and SiO_2 are consumed as CO interacts with supported Rh crystallites to produce atomically dispersed $Rh^+(CO)_2$. All these results showed the great significance of the surface properties of SiO_2 for the Rh-based catalysts, in particular the role of surface hydroxyl groups. Nevertheless, to the best of our knowledge, there have been no further reports of the effect of different surface hydroxyl groups over silica supports on the catalytic

* Corresponding author. Tel.: +86 21 6087 7221; fax: +86 21 6087 7231.
** Corresponding author at: Research Institute of Applied Catalysis, School of Chemical and Environmental Engineering, Shanghai Institute of Technology, Shanghai 201418, PR China. Tel.: +86 21 6087 7221; fax: +86 21 6087 7231.
E-mail addresses: dsmao1106@yahoo.com.cn, dsmao@sit.edu.cn (D. Mao), gzhlu@ecust.edu.cn (G. Lu).

1381-1169/$ – see front matter © 2012 Elsevier B.V. All rights reserved.
http://dx.doi.org/10.1016/j.molcata.2012.10.022

activity of Rh for CO hydrogenation. And, it is quite possible that the influences of the different kinds of hydroxyl groups on the catalytic activity of Rh-based catalysts may be different.

In this work, in order to study the role of silica surface hydroxyl groups in the synthesis of C_2 oxygenates during CO hydrogenation, different SiO_2 were employed in serving as the supports for Rh-based catalysts. Here we took a well known recipe of multi-component promoted Rh catalyst including Mn and Li [21], as a part of screening for catalysts with a high activity and selectivity of C_2 oxygenates. The catalysts were extensively characterized and evaluated for the conversion of syngas to oxygenates. Especially, the correlation between the surface hydroxyl groups on SiO_2 and catalytic performance of the Rh/SiO_2-based catalysts was discussed in detail for the first time.

2. Experimental

2.1. Catalyst preparation

SiO_2 was prepared by the Stöber method [25] as follows. The mixture solution of 21 mL tetraethylorthosilicate (TEOS) (99.5%, SCRC) and 50 mL anhydrous ethanol (99.7%, SCRC) was added slowly into the solution of 76 mL $NH_3{\cdot}H_2O$ (26 vol.%, SCRC) and 200 mL anhydrous ethanol. Then, this synthesis solution was aged for 4 h and separated centrifugally at 7000 rpm. Finally, the collected product was washed with de-ionized water for three times and dried at 70 °C for 12 h, which was denoted as SiO_2(SB). SiO_2 synthesized by the sol–gel method was denoted as SiO_2(SG). In a typical synthesis, TEOS anhydrous ethanol solution of 40 vol.% was dropped into the solution of 5 mL water, 4 g citric acid (99.5%, SCRC), and 25 mL anhydrous ethanol, under vigorous stirring at 40 °C to obtain a gel. The formed gel was dried at 90 °C for 24 h to obtain powder. The commercial SiO_2 from the Qingdao Ocean Desiccant Co, PR China, was denoted as SiO_2(CM). In order to remove the surface impurities, SiO_2(CM) was boiled in de-ionized water for 24 h and dried at 90 °C for 12 h. Before being used, all of the SiO_2 were calcined in static air at 500 °C for 6 h.

$RhCl_3$ hydrate (Rh ~ 36 wt.%, Fluka), $Mn(NO_3)_2{\cdot}6H_2O$ (99.99%, SCRC), Li_2CO_3 (99.5%, SCRC), and SiO_2 mentioned above were used in catalyst preparations. Catalysts were prepared by co-impregnation to incipient wetness of silica (1.0 g) with an aqueous solution of $RhCl_3$ hydrate and aqueous solutions of precursors of the promoters, followed by drying at 90 °C for 4 h, and then at 120 °C overnight before being calcined in air at 350 °C for 4 h. For all the catalysts, Rh loading was 1.5 wt.% and the weight ratio of Rh:Mn:Li = 1.5:1.5:0.07. The obtained catalysts are denoted as RML/SiO_2(SB), RML/SiO_2(SG) and RML/SiO_2(CM), respectively.

2.2. Reaction

CO hydrogenation was performed in a fixed-bed micro-reactor with length ~ 350 mm and internal diameter ~ 5 mm. The catalyst (0.3 g) diluted with inert α-alumina (1.2 g) was loaded between quartz wool and axially centered in the reactor tube, with the temperature monitored by a thermocouple close to the catalyst bed. Prior to reaction, the catalyst was heated to 400 °C (heating rate ~ 3 °C/min) and reduced with 10% H_2/N_2 (total flow rate = 50 mL/min) for 2 h at atmospheric pressure. The catalyst was then cooled down to 300 °C and the reaction started as gas flow was switched to a H_2/CO mixture (molar ratio of H_2/CO = 2, total flow rate = 50 mL/min) at 3 MPa. All post-reactor lines and valves were heated to 150 °C to prevent product condensation. The products were analyzed on-line (Agilent GC 6820) using a HP-PLOT/Q column (30 m, 0.32 mm ID) with detection with an FID (flame ionization detector) and a TDX-01 column with a TCD (thermal conductivity detector). The conversion of CO was calculated based on the fraction of CO that formed carbon-containing products according to: $\%\text{Conversion} = (\Sigma n_i M_i / M_{CO}) \times 100$, where n_i is the number of carbon atom in product i, M_i is the percentage of product i detected, and M_{CO} is the percentage of carbon monoxide in the syngas feed. The selectivity of a certain product was calculated based on carbon efficiency using the formula $n_i C_i / \Sigma n_i C_i$, where n_i and C_i are the carbon atom number and molar concentration of the ith product, respectively.

2.3. Catalyst characterization

The specific surface area (S_{BET}), pore volume (V_p), and pore diameter (D_p) of the samples were obtained using N_2 adsorption at −196 °C in a Micromeritics ASAP 2020 M+C adsorption apparatus. Prior to N_2 adsorption, the samples were degassed under a vacuum of 10^{-1} Pa for 10 h at 200 °C.

The X-ray powder diffraction (XRD) spectra of the samples were obtained on a PANalytical X'Pert diffractometer operating with Ni β-filtered Cu Kα (λ = 0.15418 nm) radiation at 40 kV and 40 mA. Two theta angles ranged from 10° to 85° with a scanning rate of 6 per minute. Transmission electron microscopy (TEM) images were obtained on JEM-2100 instrument operated at 200 kV.

The amount of hydrogen adsorption of various catalysts was calculated on the basis of H_2-TPD profiles. For H_2-TPD measurements, the catalyst (0.1 g) was reduced in situ for 2 h at 400 °C in 10% H_2/N_2, and then was held at 400 °C for another 30 min before being cooled down to room temperature (RT) in He flow. The next step was H_2 adsorption at RT for 0.5 h, and then the gas was swept again with He for 3 h. Subsequently, the sample was heated in a flowing He stream (50 mL/min) up to ~500 °C at a rate of 10 °C/min, while the desorbed species was detected with a TCD detector. The uptake of H_2 was used to calculate Rh metal dispersion and particle size, assuming that each surface metal atom adsorbs one H atom, i.e. $H/Rh_{surface} = 1$.

CO adsorption was studied using a Nicolet 6700 FT-IR spectrometer equipped with a DRIFT (diffuse reflectance infrared Fourier transform) cell with CaF_2 windows. The sample in the cell was pretreated in 10% H_2/N_2 at 400 °C for 2 h, and then the temperature was dropped to RT. After the cell was outgassed in vacuum to $<10^{-3}$ Pa, the background was recorded. Following by introducing CO into the IR cell ($p_{CO} = 8.0 \times 10^3$ Pa), the IR spectrum of CO adsorbed on the catalyst was recorded. Then the 10% H_2/N_2 was introduced again, and the IR spectrum of CO adsorbed was recorded at different temperatures. The concentration of CO was higher than 99.97%, and it was pretreated by dehydration and deoxygenization before being used. The spectral resolution was 4 cm^{-1} and the number of scans was 64.

CO temperature-programmed desorption (TPD) or H_2 temperature-programmed reduction (TPR) measurements were carried out in a quartz microreactor. For TPD measurements, the catalyst (0.1 g) was reduced in situ for 2 h at 400 °C in 10% H_2/N_2, followed by flushing with a He flow for 30 min at the same temperature before cooling down to RT. The next step was CO adsorption at RT for 30 min, and then the gas was swept again with He for 3 h. Subsequently, the sample was heated in a flowing He stream (50 mL/min) up to 750 °C at a rate of 10 °C/min with a quadruple mass spectrometer (QMS, Balzers OmniStar 200) as the detector to monitor the desorbed species. For TPR measurements, 0.1 g of the as-prepared sample was first pretreated at 350 °C in 20% O_2/N_2 for 1 h prior to a TPR measurement. During the TPR experiment, 10% H_2/N_2 was used at 50 mL/min and the temperature was ramped from RT to 500 °C at 10 °C/min while the effluent gas was analyzed with a TCD.

The temperature-programmed surface reaction (TPSR) experiments were carried out as follows: after the catalyst was reduced

Table 1
CO hydrogenation performance on different catalysts.

Catalyst	CO conv. (C%)	TOF[a] (s^{-1})	Selectivity of products[b] (C%)							STY(C_{2+} Oxy) (g/(kg h))
			CO_2	CH_4	MeOH	AcH	EtOH	C_{2+} Oxy[c]	C_{2+} HC[d]	
RML/SiO_2(SB)	8.2	0.068	5.3	10.3	1.7	35.5	16.5	59.1	23.6	146.8
RML/SiO_2(SG)	2.2	0.012	16.1	14.4	11.6	7.7	25.2	42.4	15.5	30.2
RML/SiO_2(CM)	6.5	0.028	17.5	11.8	5.9	15.7	18.1	37.2	27.6	80.8

Reaction conditions: T = 300 °C, P = 3 MPa, catalyst: 0.3 g, and flow rate = 50 mL/min (H_2/CO = 2), data taken after 15 h when steady state reached. Experimental error: ±5%.
[a] TOF based on CO conversion and H_2 chemisorption.
[b] Based on carbon efficiency, carbon selectivity = $n_iC_i/\Sigma n_iC_i$.
[c] C_{2+} Oxy denotes oxygenates containing two and more carbon atoms.
[d] C_{2+} HC denotes hydrocarbons containing two and more carbon atoms.

at 400 °C in 10% H_2/N_2 for 2 h, it was cooled down to RT and CO was introduced for adsorption for 0.5 h; afterwards, the H_2/N_2 mixture was swept again, and the temperature was increased at the rate of 10 °C/min with a quadruple mass spectrometer as the detector to monitor the signals of CO (m/z = 28), CO_2 (m/z = 44), and CH_4 (m/z = 15).

3. Results and discussion

3.1. Catalytic activities

Table 1 shows the catalytic activities of the Rh–Mn–Li/SiO_2 catalysts for CO hydrogenation at 300 °C. It can be seen that the activity and turnover frequency (TOF) of CO conversion over the catalysts under the same conditions decreased in a sequence: RML/SiO_2(SB) > RML/SiO_2(CM) > RML/SiO_2(SG). With respect to selectivity, the highest C_{2+} oxygenates selectivity was obtained on RML/SiO_2(SB) catalyst. The selectivity of CO_2 was similar on SiO_2(SG) and SiO_2(CM) supported catalysts, which was much higher than that on RML/SiO_2(SB) catalyst. Interestingly, formation of the undesirable by-product methane appeared to be suppressed over the RML/SiO_2(SB) catalyst, on which the methane selectivity was the lowest. Generally speaking, a higher C_{2+} oxygenates selectivity would be obtained at a lower CO conversion over the same catalyst [26]. Taking this fact into account, the C_{2+} oxygenates selectivity for the RML/SiO_2(SB) catalyst would be even more higher than those for the RML/SiO_2(CM) and RML/SiO_2(SG), if compared at the same CO conversion. Furthermore, it is noteworthy that the yield of the C_{2+} oxygenates increased remarkably from 30.2 g/(kg h) over RML/SiO_2(SG) to 146.8 g/(kg h) over RML/SiO_2(SB).

3.2. Structural and textural properties

N_2 adsorption–desorption was carried out to characterize the textural properties of the supports and the corresponding supported catalysts. As shown in Table 2, the BET surface area of SiO_2(SG) and SiO_2(CM) are 584 and 329 m^2/g, respectively. However, an extremely small BET surface area was obtained on SiO_2(SB). The value of it is only 11 m^2/g; similar surface areas of silica prepared by the Stöber method have also been reported by Szekeres et al. [25] and Hsu et al. [27]. Furthermore, for the pore distribution, SiO_2(SB) and SiO_2(CM) have a similar pore in the range of 8–9 nm, and SiO_2(SG) has a smaller pore of 2.5 nm. Upon being loaded with metal components, there was a decrease in the surface area and the pore volume for all the catalysts. In comparison, those of SiO_2(SG) decreased much heavily. It is supposed that SiO_2(SG) has a large surface area before loaded, and its pore size is just in the range of 2–3 nm, which is similar with the Rh particle size supported on SiO_2(SG) shown in Table 2. So, the larger decrease in the surface area and the pore volume of the RML/SiO_2(SG) catalyst is most likely due to pore blocking by metal particles.

X-ray diffraction (XRD) patterns (not shown) of silica and the prepared Rh–Mn–Li catalysts showed no discernable peaks related to any crystalline phase, indicating that the metal particles are highly dispersed on the SiO_2 supports due to the small content, which is consistent with the results of the dispersion and metal particle size of the catalysts shown in Table 2.

The TEM micrographs of the catalysts (not shown) indicate that the Rh particles are highly dispersed with spherical shapes, and mainly distribute in 1–5 nm. The result is consistent with those obtained by XRD and H_2 chemisorption (Table 2).

Based on the above results, it was found that although the dispersion of Rh differs among different catalysts, all of the Rh particle size on these catalysts fell in the range of 1–4 nm which is a suitable size for CO hydrogenation [5]. It has been reported that the TOF values increased with the increase in the Rh particle size over the Rh/Al_2O_3 catalyst prepared by the microemulsion technology [28]. In our case, however, the trend in TOF values of CO conversion over the catalysts does not follow that of metal particle size. On the other hand, no noticeable difference in morphology of the particles was observed by TEM measurements. These results suggest that there must be other factors rather than the size and morphology of Rh particles that affect the intrinsic site-activity (TOF) of the catalyst [26,29]. But it is still confusing that the catalyst of RML/SiO_2(SB) with the smallest BET surface area and poorest dispersion showed the highest activity and selectivity to C_{2+} oxygenates. Generally, most researches suggested that a support with a high surface area favors the dispersion of metal species, further improving the catalytic conversion of syngas to oxygenates [30]. However, some different opinions were also proposed. For instance,

Table 2
Specific surface areas (S_{BET}), pore volume (V_p) and pore diameter (D_p) from N_2 adsorption and H_2 chemisorption.

Samples	S_{BET} (m^2/g)	V_p (cm^3/g)	D_p (nm)	H_2 chemisorption		
				H_{2ads} (μmol/g)	Dispersion[a] (%)	Particle size (nm)
SiO_2(SB)	11	0.027	8.3	–	–	–
RML/SiO_2(SB)	10	0.026	7.9	25	34	3.3
SiO_2(SG)	584	0.207	2.5	–	–	–
RML/SiO_2(SG)	376	0.176	2.3	38	52	2.2
SiO_2(CM)	329	0.877	9.2	–	–	–
RML/SiO_2(CM)	321	0.828	9.0	49	67	1.7

[a] Assuming $H/Rh_{surface}$ = 1; experimental error: ±5%.

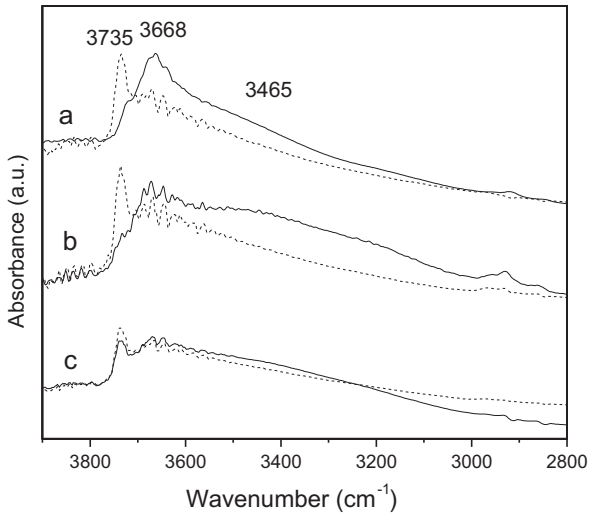

Fig. 1. FT-IR spectra of (a) SiO_2(SB) (straight) and RML/SiO_2(SB) (dash), (b) SiO_2(SG) (straight) and RML/SiO_2(SG) (dash) and (c) SiO_2(CM) (straight) and RML/SiO_2(CM) (dash) in N_2 flow at 300 °C.

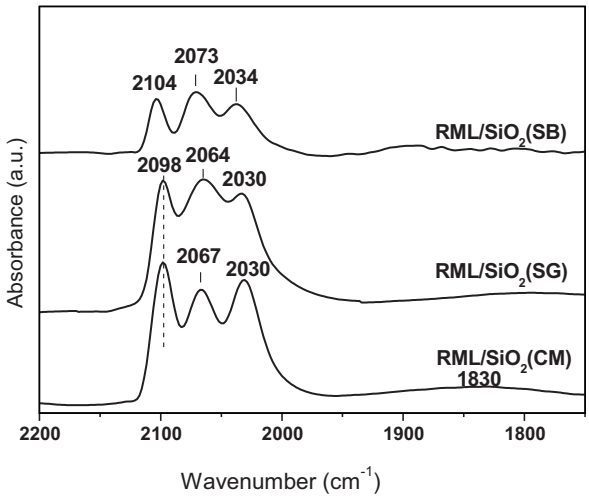

Fig. 2. FT-IR spectra of CO chemisorbed at 30 °C for 30 min.

Fan et al. [8] found that the high surface area is not the decisive factor for the dispersion of metal species in the carbon-supported Rh-based catalyst. In fact, it is suggested that the combination of the nanochannels and graphitic structure play an important role in promoting CO hydrogenation in addition to the metal dispersion in these multi-component promoted Rh catalysts. Moreover, Chen et al. [31] studied the effect of SBA-15 on Rh/Mn-supported catalysts on CO hydrogenation, and found that the catalytic performance depended on the different chemical properties of SBA-15 modified by different promoters rather than the surface areas. In this work, we also infer that there are some other properties rather than the surface area of silica, such as the role of surface hydroxyl groups on silica mentioned by many researchers [32–36], which affect the catalytic performance of the Rh–Mn–Li/SiO_2 catalysts.

3.3. FT-IR study

The IR spectra of SiO_2 and the corresponding catalysts in N_2 atmosphere at 300 °C are presented in Fig. 1. In these IR spectra, there are three main absorption regions: the first band at 3735 cm^{-1}, arises from the absorption of isolated –OH groups; the second region with peaks at 3670–3630 cm^{-1} are assigned to the weakly H-bonded OH groups; and the third region in the range 3500–2750 cm^{-1} with a maximum at 3465 cm^{-1} originates from the absorption of H_2O and strongly H-bonded OH groups [24,37].

As shown in Fig. 1, there are different intensities of the hydroxyl groups on the different silica surface. More amount of weakly H-bonded hydroxyls covers on the surface of SiO_2(SB), whereas the surface of SiO_2(SG) exhibits more amounts of strongly H-bonded hydroxyls. Compared with the supports of SiO_2(SB) and SiO_2(SG), the amount of surface hydroxyl groups on SiO_2(CM) is much lower. Furthermore, the intensity of the hydroxyl groups on SiO_2 changed obviously after supporting metal components. It can be seen that the weakly H-bonded hydroxyls over RML/SiO_2(SB) decreased and the isolated hydroxyls increased, indicating there is a metal–hydroxyl interaction. A similar variation of the strongly H-bonded hydroxyl groups was observed on RML/SiO_2(SG). However, for the RML/SiO_2(CM) catalyst, there is nearly no change in an absorption intensity of hydroxyl groups, which can be attributed mainly to a weak interaction between the metal components and hydroxyls.

In fact, a similar result was also observed by Qu et al. on Ag/SiO_2 catalysts [38]. It is suggested that the silver species could tend to interact with the H-bonded hydroxyls during the course of catalyst preparation, according to the decrease in the percentage of H-bonded hydroxyls on SiO_2 after loading silver. By combining the activities of catalysts and the above discussion, it can be inferred that the different catalytic performances of the Rh–Mn–Li catalysts supported on various SiO_2 might be related to the different hydroxyl–metal interactions.

The spectra of CO adsorbed on the in situ reduced catalysts at 30 °C for 30 min are given in Fig. 2. The IR spectrum was mainly composed by a doublet at ~2100 and ~2030 cm^{-1} and a band at around 2067 cm^{-1}. The doublet can be assigned to the symmetric and asymmetric carbonyl stretching of the gem-dicarbonyl $Rh^+(CO)_2$[CO(gdc)] and the 2067 cm^{-1} band can be attributed to the linear adsorbed CO [CO(l)] [39]. Meanwhile, the band at around 1830 cm^{-1} is assigned to the bridge bonded CO [CO(b)] [6]. It is widely accepted that the CO(l) species can be formed on the Rh^0 sites and CO(gdc) be on the Rh^+ sites which may be highly dispersed [40,41]. It can be seen from Fig. 2 and Table 3 that both the intensity of adsorbed CO and the ratio of dicarbonyl versus linear CO (Rh^+/Rh^0) on the catalysts decreased in the following order: RML/SiO_2(CM) > RML/SiO_2(SG) > RML/SiO_2(SB). This situation is similar to the reported view that a higher metal dispersion and ratio of Rh^+/Rh^0 sites were achieved with lower Si–OH density [42]. Moreover, it can be seen that the position of adsorbed CO for RML/SiO_2(SB) catalyst shifted significantly to higher frequency compared with that for other two catalysts, while the position of CO(l) for RML/SiO_2(SG) catalyst was the lowest among the three catalysts, suggesting that the Rh–CO bond strength was different caused by the different hydroxyl–metal interaction. In fact, many researchers also considered that hydroxyl groups on oxide supports can be involved in the structural rearrangement of the metal aggregates and in changes in the oxidation state of the metal [24], which can affect the CO adsorption.

In an attempt to relate the CO absorption behavior on different catalysts to their catalytic performances for CO hydrogenation, a series of infrared spectra of the in situ reduced catalysts after CO adsorption at 30 °C for 30 min followed by heating with 10% H_2/N_2

Table 3
The ratio of peak area for the adsorbed CO species.

Catalyst	RML/SiO_2(SB)	RML/SiO_2(SG)	RML/SiO_2(CM)
CO(gdc)/CO(l)[a]	1.5	1.7	2.3

[a] CO(gdc)/CO(l) denotes the peak area ratio of CO(gdc) versus CO(l) in Fig. 2; experimental error: ±5%.

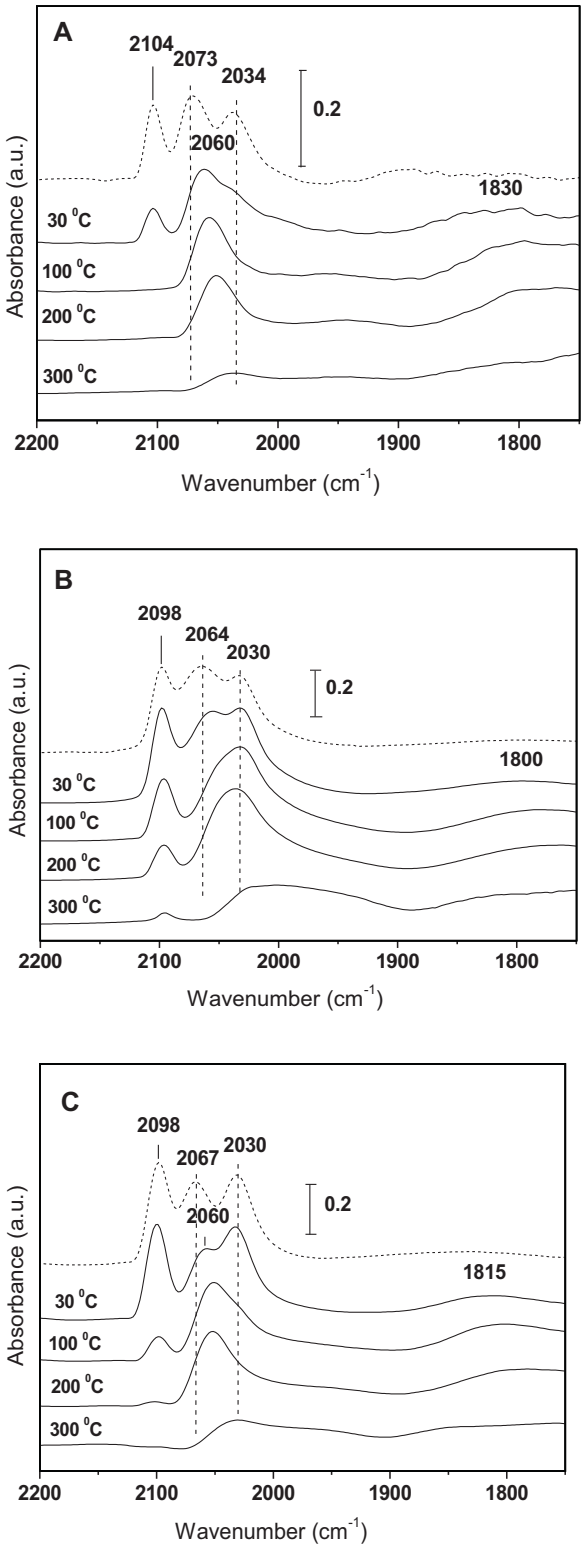

Fig. 3. FT-IR spectra of CO chemisorbed at 30 °C for 30 min (dash line) followed by heating with 10% H_2/N_2 (the straight lines): (a) RML/SiO_2(SB); (b) RML/SiO_2(SG) and (c) RML/SiO_2 (CM).

are given in Fig. 3. As observed, the CO(gdc) band on RML/SiO_2(SB) catalyst was significantly attenuated by heating to only 30 °C, and it totally disappeared followed by increase in the intensity of CO(l) species at 100 °C. During the following heating process, the position of CO(l) shifted to lower frequency, which can be interpreted by the decrease in surface coverage [11]. Its intensity fast decreased in the range of 200–300 °C. Although the spectra for the desorption behavior of adsorbed CO on RML/SiO_2(CM) catalyst was similar to that on RML/SiO_2(SB), the CO(gdc) band did not completely disappear until the temperature reached 200 °C. According to the observation that the intensity of CO(l) band would increase followed by the attenuation of CO(gdc) band, it is proposed that the Rh^+ could be reduced to Rh^0 by H_2 on RML/SiO_2(SB) and RML/SiO_2(CM) catalysts. For the RML/SiO_2(SG) catalyst, it can be seen differently that the absorption band of CO(l) strongly decreased firstly, while the CO(gdc) band was more stable in H_2 atmosphere even if at a higher temperature. Moreover, the thermal stability of the adsorbed CO species on the catalysts as a function of temperature were different, following the order as shown in Fig. 3: RML/SiO_2(SG) > RML/SiO_2(CM) > RML/SiO_2(SB).

Based on the above IR results, it is considered that the different surface properties of SiO_2 resulted in significant changes in CO adsorption species and in the intensities of CO adsorption peaks on different catalysts as a function of temperature in the presence of hydrogen: the CO(gdc) species on RML/SiO_2(SB) catalyst can be easily transformed to CO(l) species, which was consumed quickly in the reaction temperature region (200–300 °C); however, the CO(gdc) species on RML/SiO_2(SG) catalyst was stable in the H_2 atmosphere, either desorbed or reacted slowly even if in the reaction temperature region. Since it has been proved that the CO(gdc) species can be formed from CO(l) species by assisting of specific OH groups and can also be reversed to CO(l) species by H_2 addition [24], we further speculate that the interaction between weakly H-bonded OH groups on SiO_2(SB) and Rh particles weakens the Rh–CO bond strength, which is favorable for the formation of linear adsorbed CO transformed from $Rh^+(CO)_2$ species and facilitates the desorption/reactivity of the adsorbed CO. Thus, high CO conversion was obtained. The negative result came out because of the interaction between strongly H-bonded OH groups on SiO_2(SG) and Rh particles.

3.4. CO-TPD and TPSR

The desorption profiles of CO (m/z = 28) in Fig. 4(a) show that a similar associative desorption of CO took place on each catalyst, suggesting comparable strength of interaction of CO with respective catalyst surfaces. Based on the TPD results of adsorbed CO on Rh particle [43], the thermal stability of various types of adsorbed CO on Rh of the highly dispersed Rh–Mn–Li/SiO_2 catalyst is in the following order: CO(b) > CO(gdc) > CO(l). Therefore, the peak at around 105 °C should be corresponded to CO(l) species. The peak at 160 °C may be assigned to CO(gdc) species, while the peak exceeded 250 °C may be assigned to the desorption of CO(b) species or other forms [43]. Moreover, it is obvious that the desorption amount of CO(l) and CO(gdc) is consistent with the intensity of adsorbed CO discussed in Section 3.3.

Both of the signals of CO_2 (m/z = 44) and H_2 (m/z = 2) were monitored simultaneously during the CO-TPD experiment. The results are depicted in Fig. 4(b). CO_2 was observed at ~160 °C on each catalyst, and this peak is at the same temperature at which CO(gdc) species desorbed. It is suggested that CO(gdc) was desorbed in two different modes: (a) an associative desorption and (b) after being dissociated these species further react to form CO_2. Based on the amounts of CO_2 desorption at ~160 °C, it can be seen that the CO(gdc) species on RML/SiO_2(SB) catalyst was dissociated more easily than that on the other two catalysts, which may also be interpreted by the change of the Rh–CO bond strength caused by the specific hydroxyl–metal interaction.

When the desorption temperature exceeded 250 °C, the desorption peaks of CO_2 on the catalysts became broader and more complicated, and a corresponding H_2 peak was observed. It is similar to the Rh catalysts supported on Al_2O_3 and TiO_2 where the CO_2 is

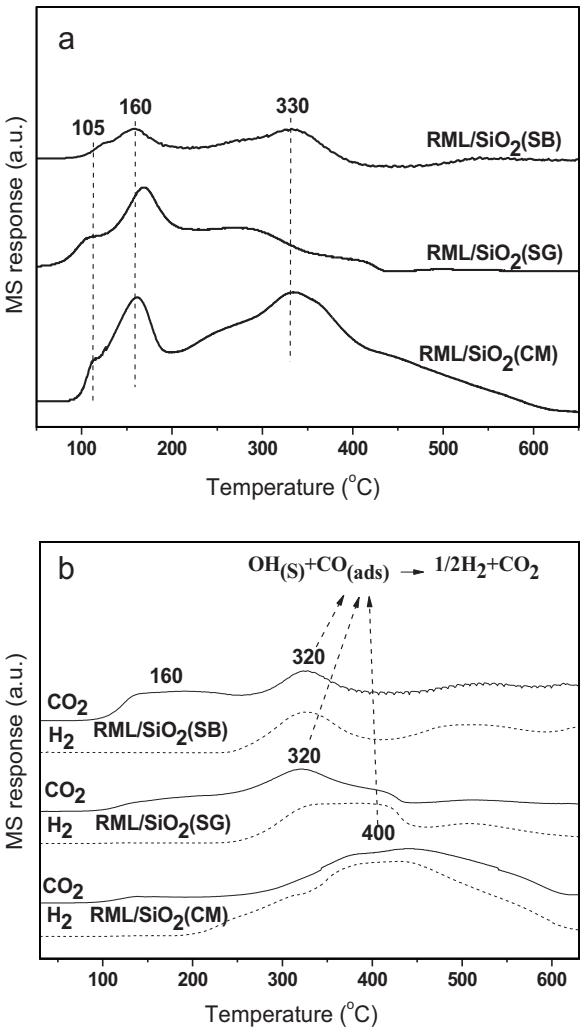

Fig. 4. Desorption profiles of CO (a) and CO_2 and H_2 (b) from CO-TPD of RML/SiO_2(SB), RML/SiO_2(SG) and RML/SiO_2(CM), after CO adsorption at room temperature.

suggested to be formed by the reaction of surface hydroxyl groups with CO species strongly adsorbed to metallic surface [44,45]:

$$CO_{(ad)} + OH_{(s)} \rightarrow CO_2 + (1/2)H_2$$

As shown in Fig. 4(b), the high-temperature CO_2 peak on RML/SiO_2(CM) was located at 400 °C, which is 80 °C higher than that on the catalysts of RML/SiO_2(SB) and RML/SiO_2(SG) (at 320 °C), suggesting that the surface hydroxyls on it could more difficultly interact with the strongly adsorbed CO due to the weak interaction between Rh particles and surface hydroxyls on SiO_2(CM).

Fig. 5 displays the TPSR profiles of the samples. It can be seen that there were two methane peaks in the profile, one was at 255 °C and the other was at around 520 °C. Although the peak location was almost the same (at 255 °C), the area of the peak for each catalyst was different: RML/SiO_2(SG) had the strongest intensity of CH_4 peak; on the contrary, the smallest peak of CH_4 was shown on RML/SiO_2(SB). According to the viewpoint of Chen et al. [31], this observation indicates that the number of active sites responsible for methane production decreased in the following order: RML/SiO_2(SG) > RML/SiO_2(CM) > RML/SiO_2(SB), which is in line with the CH_4 selectivity over the catalysts. In addition, the broad peak centered at 520 °C might be due to the hydrogenation of carbon species formed at lower temperatures and transformed to a less active form [43].

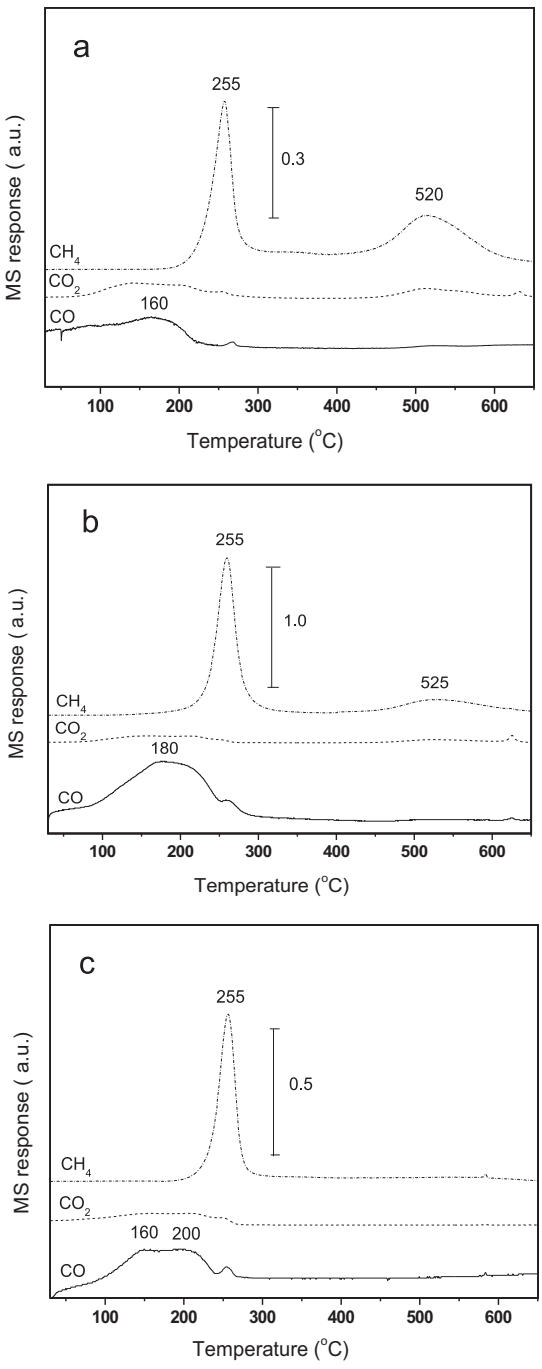

Fig. 5. CO, CO_2 and CH_4 desorption from TPSR of RML/SiO_2(SB) (a), RML/SiO_2(SG) (b) and RML/SiO_2(CM) (c), following continuous CO adsorption at room temperature.

By combining the results of CO-TPD with TPSR, it is obvious that CH_4 is formed at the expense of the strongly adsorbed CO species, and most of them come from the CO(b) species and part of adsorbed CO could transform to CO_2 at a high temperature (above 250 °C) in the absence of H_2. The desorption peak of CO below 250 °C in TPSR was also different from CO-TPD; only a broad peak between 100 °C and 250 °C left on these catalysts. Compared with the catalysts of RML/SiO_2(SB) and RML/SiO_2(CM), the biggest peak at ~160 °C attributed to the desorption of CO(gdc) species was kept on RML/SiO_2(SG) catalyst, which is consistent with the desorption behavior of the adsorbed CO in the presence of H_2 observed by IR. This result also proved that H_2 spillover might occur on the catalysts at the low temperature [46] and the

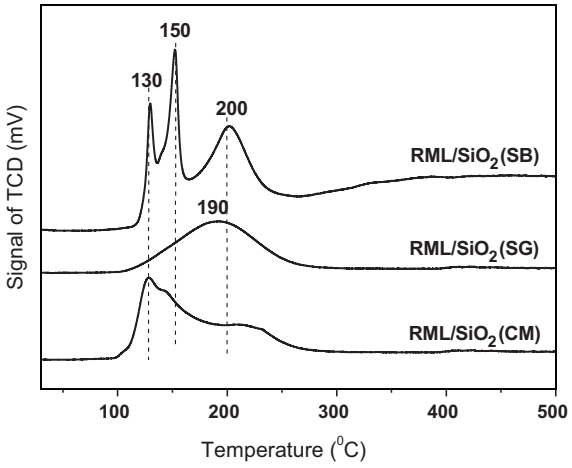

Fig. 6. TPR profiles of the catalysts.

adsorbed CO with different bond strength caused by the various hydroxyl–metal interactions could be desorbed by different behaviors. Nevertheless, one contradiction should be noted here that the highest amount of CH_4 was formed on RML/SiO_2(SG) which had the least amount of CO(b) species. It may be concluded that the boosting of hydrogenation at a certain temperature (255 °C) would cause the adsorbed CO to dissociate and form CH_4, if the adsorbed CO still adsorbs on the metallic surface at that temperature.

3.5. H_2-TPR

Fig. 6 shows the temperature programmed reduction (TPR) profiles for all the catalysts. There were three distinct peaks of H_2 consumption in the TPR profile of RML/SiO_2(SB) catalyst. According to the previous results, the high temperature peak centered at 200 °C is ascribed to the reduction of MnO_2 [10,44]. The peaks at 130 °C and 150 °C are ascribed to the reduction of Rh_2O_3 not intimately contacting with Mn species (denoted as Rh(I)) and of Rh_2O_3 intimately contacting with Mn species (denoted as Rh(II)), respectively [47,48]. The sample of RML/SiO_2(CM) also had three peaks which are similar to RML/SiO_2(SB), but the reduction peak of Rh(II) shifted to a lower temperature and the reduction peak of MnO_2 shifted to a higher temperature compared with that of RML/SiO_2(SB). Moreover, the sample of RML/SiO_2(SG) only showed a wide peak centered at 190 °C, which pointed to a strong interaction between Rh_2O_3 and Mn species. According to the viewpoint proposed by Chen et al. [49], it is suggested that a moderate Rh–Mn interaction is favorable for production of C_{2+} oxygenates.

On basis of the H_2-TPR, FT-IR, and catalytic test results, we propose the following model to explain the different catalytic performances of Rh–Mn–Li/SiO_2 via different hydroxyl–metal interactions. It is conceivable that SiO_2(CM) has less hydroxyl groups to interact with the metal species, resulting in a weak Rh–Mn interaction on RML/SiO_2(CM) catalyst. Compared with the SiO_2(CM) supported catalyst, the interaction between weakly H-bonded hydroxyl groups on SiO_2(SB) and metal particles could achieve a moderate contact between Rh and Mn, which is conducive to the transformation of CO(gdc), and finally resulting in the high CO conversion and selectivity of C_{2+} oxygenates. In contrast, the effect of strongly H-bonded associated hydroxyl groups on RML/SiO_2(SG) enhances the Rh–Mn interaction, which suppresses the transformation of CO(gdc), finally inhibits the CO conversion and formation of C_{2+} oxygenates.

4. Conclusions

The direct synthesis of ethanol and other oxygenates from CO hydrogenation over Rh–Mn–Li/SiO_2 catalysts depended greatly on the properties of SiO_2. Different activity and selectivity of C_{2+} oxygenates were obtained on different SiO_2-supported Rh–Mn–Li catalysts. Results from FT-IR confirmed that various surface hydroxyl groups exist on the supports, and interact differently with the metal particles. Based on the result of H_2-TPR, it is further proved that the original hydroxyl groups on the supports have different interactions with metal particles, which finally affects the Rh–Mn interaction. The IR spectra of CO adsorption indicated that the linear Rh–CO is the more active adsorbed species for CO hydrogenation. In addition, the results suggest that the effect of weakly H-bonded hydroxyl groups is favorable to transform CO(gdc) to CO(l) species and facilitate the desorption/reactivity of the CO(l) species, finally resulting in high CO conversion and selectivity of C_{2+} oxygenates over the RML/SiO_2(SB) catalyst. Overall, the different Rh–Mn interaction intensity, which is caused by the reaction of metal (Rh and Mn) with different hydroxyl groups on the surface of various SiO_2 supports, plays a crucial role in deciding the activity and selectivity of the Rh–Mn–Li/SiO_2 catalyst for CO hydrogenation.

Acknowledgments

The authors gratefully acknowledge financial support from the Science and Technology Commission of Shanghai Municipality (08520513600), Leading Academic Discipline Project of Shanghai Education Committee (J51503) and Shanghai Institute of Technology (KJ2011-02). The linguistic revisions of the manuscript provided by the anonymous reviewers are also gratefully acknowledged.

References

[1] V. Subramani, S.K. Gangwal, Energy Fuels 22 (2008) 814–839.
[2] J.J. Spivey, A. Egbebi, Chem. Soc. Rev. 36 (2007) 1514–1528.
[3] J.R. Rostrup-Nielsen, Science 308 (2005) 1421–1422.
[4] D.H. Mei, R. Rousseau, S.M. Kathmann, V.A. Glezakou, M.H. Engelhard, W.L. Jiang, C.M. Wang, M.A. Gerber, J.F. White, D.J. Stevens, J. Catal. 271 (2010) 325–342.
[5] T. Hanaoka, H. Arakawa, T. Matsuzaki, Y. Sugi, K. Kanno, Y. Abe, Catal. Today 58 (2000) 271–280.
[6] A.C. Yang, C.W. Garland, J. Phys. Chem. 61 (1957) 1504–1512.
[7] J.P. Hindermann, G.J. Hutchings, A. Kiennemann, Catal. Rev.-Sci. Eng. 35 (1993) 1–127.
[8] Z.L. Fan, W. Chen, X.L. Pan, X.H. Bao, Catal. Today 147 (2009) 86–93.
[9] S.S.C. Chuang, R.W. Stevens Jr., R. Khatri, Top. Catal. 32 (2005) 225–232.
[10] H.Y. Luo, P.Z. Lin, S.B. Xie, H.W. Zhou, C.H. Xu, S.Y. Huang, L.W. Lin, D.B. Liang, P.L. Yin, Q. Xin, J. Mol. Catal. A: Chem. 122 (1997) 115–123.
[11] X. Mo, J. Gao, J.G. Goodwin Jr., Catal. Today 147 (2009) 139–149.
[12] J. Gao, X. Mo, A.C. Chien, W. Torres, J.G. Goodwin Jr., J. Catal. 262 (2009) 119–126.
[13] X. Mo, J. Gao, N. Umnajkaseam, J.G. Goodwin Jr., J. Catal. 267 (2009) 167–176.
[14] N.D. Subramanian, J. Gao, X. Mo, J.G. Goodwin Jr., W. Torres, J.J. Spivey, J. Catal. 272 (2010) 204–209.
[15] M. Ojeda, M.L. Granados, S. Rojas, P. Terreros, F.J. García- García, J.L.G. Fierro, Appl. Catal. A: Gen. 261 (2004) 47–55.
[16] Z.L. Zhang, A. Kladi, X.E. Verykios, J. Catal. 156 (1995) 37–50.
[17] J.A. Anderson, M.M. Khader, J. Mol. Catal. A: Chem. 105 (1996) 175–183.
[18] J.C. Lavalley, J. Saussey, J. Lamotte, R. Breault, J.P. Hindermann, A. Kiennemann, J. Phys. Chem. 94 (1990) 5941–5947.
[19] R. Burch, M.J. Hayes, J. Catal. 165 (1997) 249–261.
[20] S. Ho, Y. Su, J. Catal. 168 (1997) 51–59.
[21] W.M. Chen, Y.J. Ding, D.H. Jiang, Z.D. Pan, H.Y. Luo, Catal. Lett. 104 (2005) 177–180.
[22] D.H. Jiang, Y.J. Ding, Z.D. Pan, W.M. Chen, H.Y. Luo, Catal. Lett. 121 (2008) 241–246.
[23] F. Solymosi, I. Tombacz, M. Kocsis, J. Catal. 75 (1982) 78–93.
[24] P. Basu, D. Panayotov, J.T. Yates Jr., J. Am. Chem. Soc. 110 (1988) 2074–2081.
[25] M. Szekeres, O. Kamalin, P.G. Grobet, R.A. Schoonheydt, K. Wostyn, K. Clays, A. Persoons, I. Dkénáy, Colloids Surf. A: Physicochem. Eng. Aspects 227 (2003) 77–83.
[26] S. Ito, S. Ishiguro, K. Nagashima, K. Kunimori, Catal. Lett. 55 (1998) 197–199.
[27] W.P. Hsu, R.C. Yu, E. Matijevic, J. Colloid Interface Sci. 156 (1993) 56–65.

[28] M. Ojeda, S. Rojas, M. Boutonnet, F.J. Pérez- Alonso, F.J. García- García, J.L.G. Fierro, Appl. Catal. A: Gen. 274 (2004) 33–41.
[29] T. Tago, T. Hanaoka, P. Dhupatemiya, H. Hayashi, M. Kishida, K. Wakabayashi, Catal. Lett. 64 (2000) 27–31.
[30] L. Guzzi, Z. Schay, K. Matusek, I. Bogyay, Appl. Catal. 22 (1986) 289–309.
[31] G.C. Chen, C.Y. Guo, X.H. Zhang, Z.J. Huang, G.Q. Yuan, Fuel Process Technol. 92 (2011) 456–461.
[32] A. Brenner, D.A. Hucul, J. Catal. 61 (1980) 216–222.
[33] D.A. Hucul, A. Brenner, J. Phys. Chem. 85 (1981) 496–498.
[34] A.K. Smith, F. Hugues, A. Theolier, J.M. Basset, R. Ugo, G.M. Zanderighi, J.L. Bilhon, V. Bilhou-Bougnal, W.F. Graydon, Inorg. Chem. 18 (1979) 3104–3112.
[35] F. Solymosi, M. Pasztor, J. Phys. Chem. 89 (1985) 4789–4793.
[36] F. Solymosi, M. Pasztor, J. Phys. Chem. 90 (1986) 5312–5317.
[37] J.B. Peri, J. Phys. Chem. 70 (1966) 2937–2945.
[38] Z.P. Qu, W.X. Huang, S.T. Zhou, H. Zheng, X.M. Liu, M.J. Cheng, X.H. Bao, J. Catal. 234 (2005) 33–36.
[39] S.D. Worley, G.A. Mattson, R. Caudlll, J. Phys. Chem. 87 (1983) 1671–1673.
[40] R.R. Cavanagh, J.T. Yates Jr., J. Chem. Phys. 74 (1981) 4150–4155.
[41] C.A. Rice, S.D. Worley, C.W. Curtis, J.A. Guin, A.R. Tarrer, J. Chem. Phys. 74 (1981) 6487–6497.
[42] S.L. Guo, M. Arai, Y. Nishiyama, Appl. Catal. 65 (1990) 31–44.
[43] Y. Wang, H.Y. Luo, D.B. Liang, X.H. Bao, J. Catal. 196 (2000) 46–55.
[44] T. Ioannides, X. Verykios, J. Catal. 140 (1993) 353–369.
[45] A. Egbebi, V. Schwartz, S.H. Overbury, J.J. Spivey, Catal. Today 149 (2010) 91–97.
[46] Y. Wang, Z. Song, D. Ma, H.Y. Luo, D.B. Liang, X.H. Bao, J. Mol. Catal. A: Chem. 149 (1999) 51–61.
[47] D.H. Jiang, Y.J. Ding, Z.D. Pan, X.M. Li, G.P. Jiao, J.W. Li, W.M. Chen, H.Y. Luo, Appl. Catal. A: Gen. 331 (2007) 70–77.
[48] H.M. Yin, Y.J. Ding, H.Y. Luo, H.J. Zhu, D.P. He, J.M. Xiong, L.W. Lin, Appl. Catal. A: Gen. 243 (2003) 155–164.
[49] W.M. Chen, Y.J. Ding, H.Y. Luo, L. Yan, T. Wang, Z.D. Pan, H.J. Zhu, Chin. J. Appl. Chem. 22 (2005) 470–474.